ADVANCED FUNCTIONAL MATERIALS
www.afm-journal.de

Transparent, Highly Stretchable, Rehealable, Sensing, and Fully Recyclable Ionic Conductors Fabricated by One-Step Polymerization Based on a Small Biological Molecule

*Chao Dang, Ming Wang, Jie Yu, Yian Chen, Shenghui Zhou, Xiao Feng, Detao Liu, and Haisong Qi**

To date, various stretchable conductors have been fabricated, but simultaneous realization of the transparency, high stretchability, electrical conductivity, self-healing capability, and sensing property through a simple, fast, cost-efficient approach is still challenging. Here, α-lipoic acid (LA), a naturally small biological molecule found in humans and animals, is used to fabricate transparent (>85%), electrical conductivity, highly stretchable (strain up to 1100%), and rehealable (mechanical healing efficiency of 86%, electrical healing efficiency of 96%) ionic conductor by solvent-free one-step polymerization. Furthermore, the ionic conductors with appealing sensitivity can be served as strain sensors to detect and distinguish various human activities. Notably, this ionic conductor can be fully recycled and reprocessed into new ionic conductors or adhesives by a direct heating process, which offers a promising prospect in great reduction of electronic wastes that have brought acute environmental pollution. In consideration of the extremely facile preparation process, biological available materials, satisfactory functionalities, and full recyclability, the emergence of LA-based ionic conductors is believed to open up a new avenue for developing sustainable and wearable electronic devices in the future.

1. Introduction

Stretchable conductors have drawn enormous consideration attributed to its significantly flexible, lightweight, and sensory features.[1–4] These conductors provide huge opportunities for promising applications of artificial muscles, skin sensors, biological actuators, stretchable displays, electronic eye cameras, intelligent robot arms, and others.[5–11] It was well known that the conventional electronic conductors are normally prepared from wafer-based materials, which possess several drawbacks including fragility, rigidity, and low conductivity under large-scale deformations.[12] They cannot satisfy the demands of high stretchability, flexibility, durability, and stability. To achieve these criteria, strain engineering and nanocomposites are the two most adoptable strategies to fabricate stretchable conductors. In the first strategy, nonstretchable inorganic materials, such as silicon and metals, are geometrically patterned into buckled, serpentine structures on elastomeric substrates that renders the conductors excellent sensitivity and larger workable range of strain.[10,13,14] Nonetheless, most resultant conductors still show narrow range of strain from 20% to 70%,[15] and presents out-of-plane patterns that is difficult to encapsulate. Meanwhile, this strategy usually involves expensive and very complicated techniques, which greatly limits the further development of these conductors. Integrating conductive fillers into polymer matrix to produce nanocomposites used as stretchable conductors is the second strategy.[16] So far, various nanomaterials, such as carbon nanotubes,[17–20] carbon black,[21] graphene-based materials,[22,23] metal nanowires, and nanoparticles,[24,25] have been used as conductive fillers because of their unique mechanical and electrical properties. Although the robustness, stretchability, and sensitivity of such conductors are greatly enhanced, their large-scale applications are still restricted by several challenging issues. For example, embedding nanomaterials into polymer matrix usually cause soft-hard material interfacial failure. Besides, the poor transparency hinders their application in touch screens and biomedical imaging. Additionally, the expensive nanomaterials, relative complicated, and time-consuming fabrication processes are also significant limiting factors toward the application of these stretchable conductors.[26,27]

Dr. C. Dang, Dr. M. Wang, Dr. J. Yu, Dr. S. Zhou, Dr. X. Feng, Prof. D. Liu, Prof. H. Qi
State Key Laboratory of Pulp and Paper Engineering
South China University of Technology
Guangzhou 510641, China
E-mail: qihs@scut.edu.cn
Dr. Y. Chen
Leibniz-Institut für Polymerforschung Dresden e. V. (IPF)
Hohe Straße 6, 01069 Dresden, Germany
Dr. Y. Chen
Organic Chemistry of Polymers
Technische Universität Dresden
01062 Dresden, Germany
Prof. H. Qi
Guangdong Engineering Research Center for Green Fine Chemicals
Guangzhou 510640, China
The ORCID identification number(s) for the author(s) of this article can be found under https://doi.org/10.1002/adfm.201902467.

DOI: 10.1002/adfm.201902467

Ionic conductors, combination of intrinsic stretchability, self-healing, and transparency,[28–32] have aroused the extensive interest of many researchers. Chen co-workers reported a rubber band like conductors based on ionic liquid, which can be assembled into wearable sensors to real-time detection of human health.[33] Wang and Yang et al developed ionic hydrogels with self-healing capability, high stretchability and transparency, and assembled it into strain sensors to measure human activities.[34] However, the commonly used ionogel is made of ionic liquid, which consists of expensive component, requires complex fabrication process, and is harmful to the environment. It should be noted that the water in hydrogel based conductors would evaporate gradually when they are exposed to open air. This can make these materials easily dry out in practical uses thus leading to an unsatisfactory user experience.[35] Furthermore, the complicated polymerization process still remains a major challenge to prepare ionic conductors.

As naturally small biological molecule existed in human and animals, α-lipoic acid (LA) is biodegradable and biocompatible. It plays a crucial role in aerobic metabolism,[36] and can be used as drugs or supplements for stress-related diseases, diet, diabetes, and antiaging. Due to the existence of disulfide bond in LA molecular structure, the thermal-initiated ring-opening polymerization can be easily realized by dynamic disulfide exchange,[37] thus obtaining clear molten liquid consisting of primary linear covalent backbones (Figure S1, Supporting Information). After cooling, the formation of hydrogen bonds between carboxyl groups of LA can efficiently self-crosslink the linear poly (LA), resulting in transparent and yellow solid polymers. This special molecular structure renders it unique tailored properties, which have great potential in construction of functional materials.[38] Unfortunately, LA always suffers from the inverse ring-closing depolymerization, which makes the transparent yellow polymers turn into opaque and rigidity after a few minutes (Figure S2, Supporting Information).[39]

Herein, we report a novel LA-based ionic conductor by a heating process with acrylic acid (AA), choline chloride (CCl), and ferric chloride (Fe^{3+}). The solvent-free process is extremly facile, fast, low-cost, and scalable. Interestingly, the transparent, highly stretchable, and rehealable properties are achieved simultaneously for our ionic conductor owing to the collective contribution from disulfide bonds, hydrogen bonds, and coordination bonds. In addition, this ionic conductor shows appealing sensitivity as strain sensors, which can be directly mounted on human body to detect and distinguish various human motions. It is worth noting that our ionic conductors can be fully recycled and reprocessed into new ionic conductors or adhesives by a direct heating process and thus is very low-cost, fast, and ecofriendly.

2. Results and Discussion

2.1. Material Synthesis and Characterization

The facile heating process to functionalize LA is shown in **Figure 1** and Figure S3 (Supporting Information). AA, CCl, and Fe^{3+} were firstly added into the molten LA liquid at 90 °C for 30 min under vigorous stirring to form clear and yellow solution. Then cooling it to room temperature to obtain the solid, transparent, and soft polymer composite. As the Raman spectra shown in Figure S4 (Supporting Information), the peak at 510 cm^{-1} attributed to disulfide bonds split into two pronounced peaks at 508 and 525 cm^{-1}, which verified the ring opening polymerization of LA.[37] Moreover, the appearance of new peak at 673 cm^{-1} related to C-S bonds demonstrated the realization of addition polymerization between AA and terminal diradicals

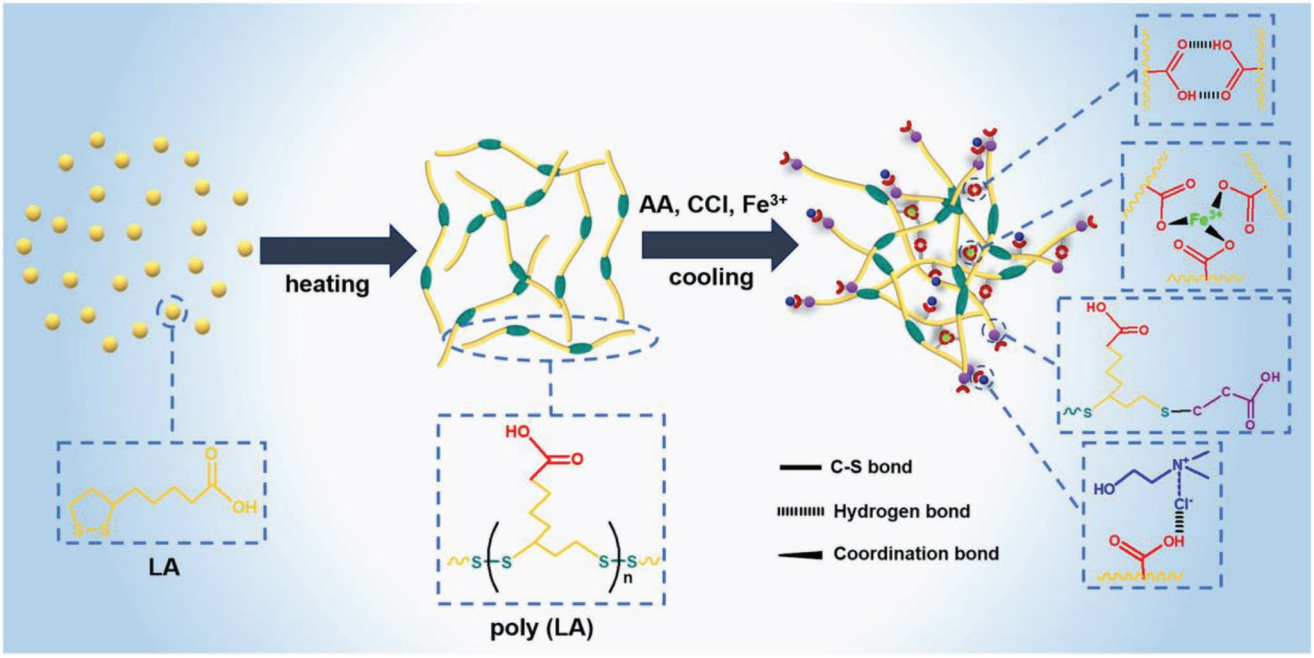

Figure 1. Schematic diagram of the polymerized process for the polymer composites and the corresponding interactions between poly (LA) chains with acrylic acid, choline chloride, and ferric chloride.

of poly (LA).[38] Based on the Fourier transform infrared spectroscopy (FT-IR) spectrum of the resultant polymer composite (Figure S5, Supporting Information), the observed changes of characteristic peaks (the reduced peak at 1714 cm^{-1}, increased peak at 3326 cm^{-1}, shifted peak at 622 cm^{-1}, and new peak at 1624 cm^{-1}) could indicate the formation of hydrogen bonds, C-S bonds, and Fe^{3+}-carboxylated coordinative bonds in the polymer networks.[38,40] Moreover, new shoulder-like absorption peaks in the range of 342–348 nm were detected in UV–vis absorption spectrums (Figure S6, Supporting Information), further revealing the formation of coordination bonds.[41]

Based on the results mentioned above, the formation of the polymer composite can be described as a schematic diagram as Figure 1. That is, LA monomers were first heated to form primary linear covalent backbones linked by dynamic disulfide bonds. Then, the double bond of AA was added to the terminal diradicals of these backbones, which could inhibit the inverse ring-closing depolymerization of LA. Meanwhile, the linked AA could offer additional carboxyl groups to form hydrogen bonds with LA polymer chains, further increasing the mechanical performances. Due to the good hydrogen bonds accepting ability and favorable electrical property,[42,43] CCl could also form hydrogen bonds with carboxylic groups, endowing the polymer composites with ionic conductivity. After introduction of Fe^{3+}-carboxylated coordinative bonds, the hierarchical polymer network consisting of dynamic disulfide bonds, hydrogen bonds, and coordination bonds was successfully obtained.[44] Additionally, both the thermogravimetry (TG) and differential scanning calorimeter (DSC) analysis (Figures S7, S8 and Table S1, Supporting Information) demonstrated that this material possessed higher thermal stability, further indicating the complex polymer networks were formed during this polymerization.[45] Figure S9 (Supporting Information) gives the surface scanning electron microscopy (SEM) image of the polymer composite. They further demonstrated the existence of a continuous, high density homogenous phase without obvious holes in the polymer composite.

2.2. Transparent, Conductive, and Mechanical Performances

Besides the structural characteristics of the polymer composite, their functionalities in optics, electricity, and mechanics were investigated comprehensively. As shown in **Figure 2**a, the polymer composite with 1.5 mm thickness exhibited good transparency. Notably, the transparency of this material was depended on the content of Fe^{3+} (Figure 2a and Figure S10, Supporting Information). With an increase of Fe^{3+} ions from 0.02% to 0.5%, the transparency values of samples decreased gradually from 90% to 67% (Figure S11, Supporting Information). The main cause of transmittance reduction is the color of Fe^{3+} ions. On the other hand, the extensive coordination bonding interactions would lead to the formation of more complex polymer networks, which could also block the light passing through them.[29] In addition, the transmittance showed declining trend with the increased thickness of the resultant polymer composite (Figure S12, Supporting Information).

The photograph in Figure 2b presents the ionic conductivity of the polymer composite. This is because the positive/negative ions of CCl could freely move in the polymer networks under the exterior electric field. The electrical properties were measured by electrochemical impedance spectroscopy (ESI). The electrical conductivity exhibited strong dependence on Fe^{3+} content (Figure 2b; Figure S13, Supporting Information). With an increase of Fe^{3+} content from 0.02% to 0.5%, the conductivity decreased from 2.4×10^{-3} to 1.4×10^{-3} S m^{-1}. The incorporation of Fe^{3+} into the polymer system could endow the polymer composite with more complex crosslinked networks, which could hinder the free movement of ions in polymer networks. Thus, the influence of Fe^{3+} on electrical conductivity was negative. As mentioned above, CCl could act as hydrogen-bond acceptor to introduce the positive/negative ions in polymer system, crucial for the promotion of ionic conductivity. Therefore, by tuning the weight ratio of LA and CCl, a series of polymer composites with different electrical conductivity is obtained. As shown in Figure S14 (Supporting Information), when increasing the content of CCl up to 40 wt%, this composite presented a higher electrical conductivity of 2.8×10^{-3} S m^{-1}. However, further increasing the CCl content would hinder the formation of Fe^{3+}-carboxylated coordinative bonds, resulting in the poor mechanical strength of this material.

Apart from the high transparency and ionic conductivity, this material exhibited outstanding mechanical strength. Rheological analysis of the polymer composite indicated the storage modulus (G') was predominate and obviously higher than the loss modulus (G'') (Figures S15 and S16, Supporting Information), suggesting the elastic solid behavior of this materials.[46] With increasing Fe^{3+} from 0.02 to 0.5 mol%, the G' and G'' of the polymer composite were enhanced obviously, which suggested the positive effect of coordination bonds on the strength of polymer networks.[47] Besides, the G'' displayed a slight reduction with an increment of shear strain, which may be related to the disassociation of disulfide bonds, hydrogen bonds, and coordination bonds in the polymer network. This polymer composite was further demonstrated to withstand cutting and compressing, which exhibited excellent mechanical strength (Figure S17, Supporting Information). Moreover, the composite could be stretched into 11 times its initial dimension without breaking (Figure 2c). From the stress–strain curves in Figure 2d, the polymer composite without Fe^{3+} just exhibited a stretchability of 723% with low stress of 47 kPa, while that with 0.3% Fe^{3+} showed the increased stretchability of 1092% with high tensile stress of 152 kPa. The corresponding Young's modulus displayed obvious enhancement with the increasing Fe^{3+} content, indicating the significant contributions of coordinate bonds to the mechanical properties (Figure S18, Supporting Information). Furthermore, the reversibility of the materials was also investigated by the cyclic tensile tests (Figures S19 and S20, Supporting Information). It could be found that the polymer composite showed a larger hysteresis loop with larger strains during the cyclic tensile. This result indicated that the composites possessed more effective pathway to dissipate lots of energy. The fatigue resistance experiments demonstrated that the polymer composite could remain nearly constant after 20 successive stretching–releasing cycles with a strain of 100% (Figure S21, Supporting Information).

Combining the above evidences, the proposed mechanism resulting in the excellent properties was schematically illustrated in Figure 2e. On one hand, the presence of irregularly

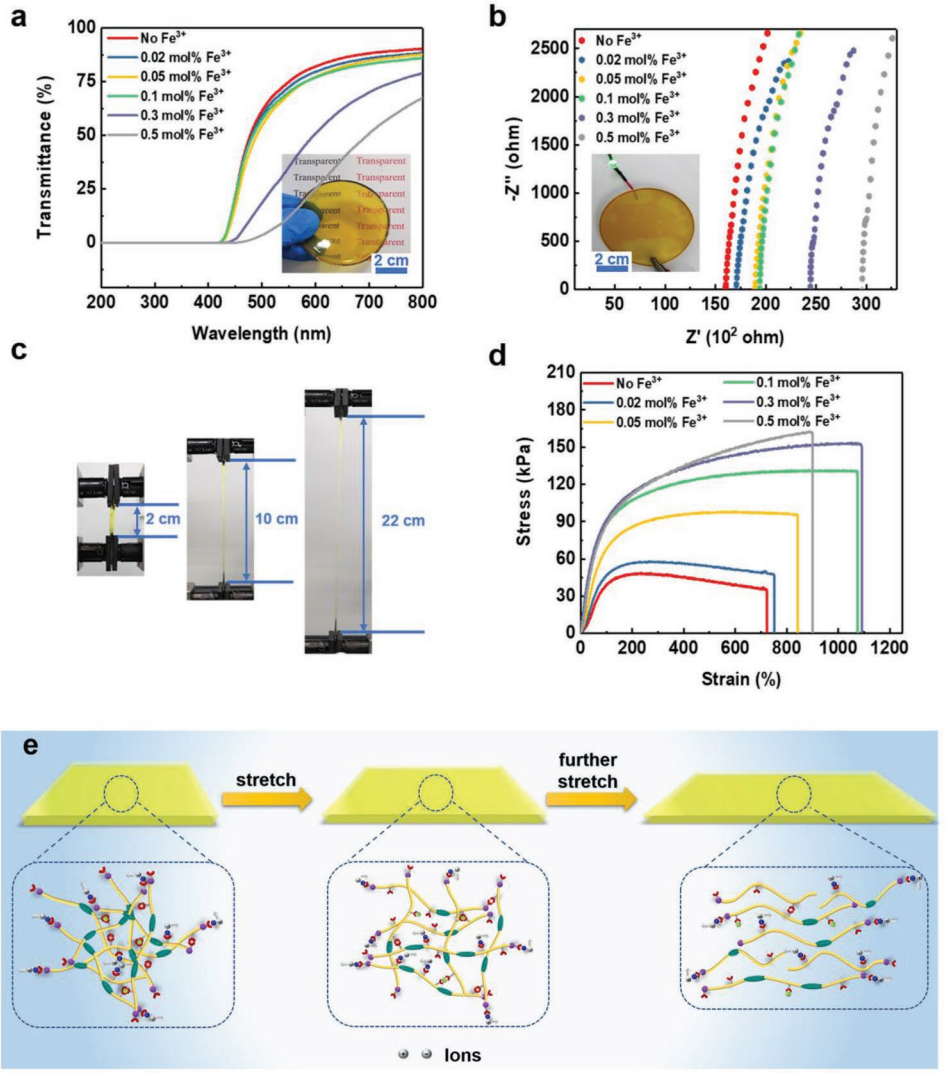

Figure 2. Transparent, conductive, and mechanical performances of the polymer composites. a) UV spectrum. b) Electrochemical impedance spectroscopy (EIS) plots. c) Digital images of the polymer composite with 0.1 mol% Fe^{3+} by uniaxial tensile test. d) Typical strain stress curves. e) Energy dissipation mechanism of the polymer composite network under ultrahigh stretchability.

arranged polymer networks caused an amorphous medium. Thus the light could easily go through the composite matrix, leading to the high transmittance of this material.[29] On the other hand, the as-formed dynamic chemical bonds, such as disulfide bonds, hydrogen bonds, and coordination bonds, could be hierarchically broken and rebonded upon continuous strain by a efficient energy dissipation mechanism.,[48,49] thus endowing ultrahigh stretchability in the polymer composites.

2.3. Self-Healing Performances

The self-healing performances in mechanical strength and electrical conductivity were investigated, respectively. As displayed in **Figure 3**a, two cut-off polymer composite films autonomously healed under room temperature after 14 h without using any healing agent and external stimulus. The healed composite film was strong enough to bend and lift a 200 g weight without tearing. As shown in Figure 3b, the fracture stress of the healed polymer composite was significantly enhanced with an increase of healing time. The corresponding healing efficiency obviously increased from 30% to 86% with the healing time increased from 0.2 to 14 h (Figure 3c), indicating this materials possess good mechanical self-healing capability. Furthermore, it is noted that the healing efficiency could be greatly enhanced by increasing Fe^{3+} content. It demonstrated the crucial role of coordination bonds for the self-healing capability of our polymer composites. The self-healing feature of the polymer composites in electrical conductivity was further investigated. Figure 3d shows the real-time resistance variation of the polymer composite during the cutting-healing processes. When the sample was cut apart, the resistance of the material increased rapidly to infinity due to the conductive pathway failed. Once the two separate parts were put together, the conductive pathway was rapidly recovered and the resistance dropped accordingly within 1.5 s (Figure S22, Supporting

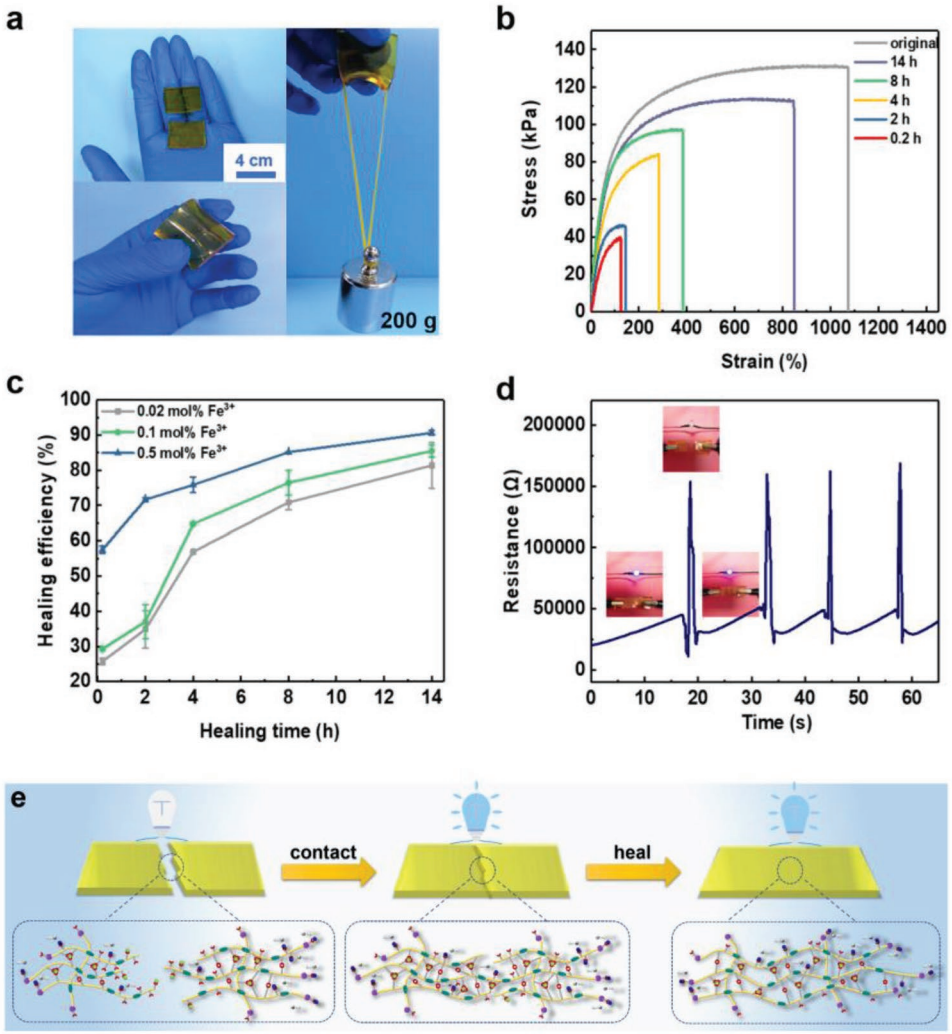

Figure 3. Self-healing performances of the polymer composites. a) Photograph of the self-healing process (polymer composite with 0.1 mol% Fe^{3+} was cut and then re-healed for 14 h at 25 °C). b) Tensile stress–strain curves of the original and self-healed polymer composites with 0.1 mol% Fe^{3+} under different healing time. c) Healing efficiency versus healing test time of the polymer composites. d) Resistance versus test time during the cyclic break-healing process for the polymer composite with 0.1 mol% Fe^{3+}. e) Schematic diagram of possible self-healing mechanism for the polymer composites.

Information). After the first cutting-healing cycle, the resistance of the composite was 21 215 Ω, which recovered to 96% of its initial value. Even after four successive cutting-healing cycles, the resistance of this material could almost recover to its original value (Figure S23, Supporting Information). These observations indicated that the polymer composites possessed high self-healing efficiency and fast, stable electrical self-healing capability.

The mechanism of the superior self-healing performances was illustrated in Figure 3e. During the self-healing process, the hydrogen bonds and coordination bonds was first recombined by assistance of the LA molecular chain segments movement,[50] thus resulting in the quick restoration of the conductive pathway.[51] Hence, the healing ability of electrical conductivity is much higher than that of mechanical performances. Then, the dynamic disulfide bonds further recombined along the migration direction of polymer chains, well facilitating the reconstruction of the polymer networks.[52,53] Based on the above studies, this transparent, conductive, highly stretchable, and rehealable polymer composite is perfectly suitable to be used as ionic conductor for various functional applications.

2.4. Strain Sensitivity

The strain sensitivity of the polymer composites under a loading process was intuitively illustrated by integrating the composite into a complete circuit connecting a blue LED indicator (**Figure 4**a). The LED became increasingly dimmed with the increasing of strain, which indicated the good response ability to the applied strain on our composite. The correlation of electrical resistance changes and mechanical strain of the polymer composite was also quantitatively investigated. As shown in Figure 4a, the material displays a linear increase in relative resistance changes with a maximal strain up to 300%. The gauge factors are 1.46 within 50% strain, 2.30 within 150% strain, and

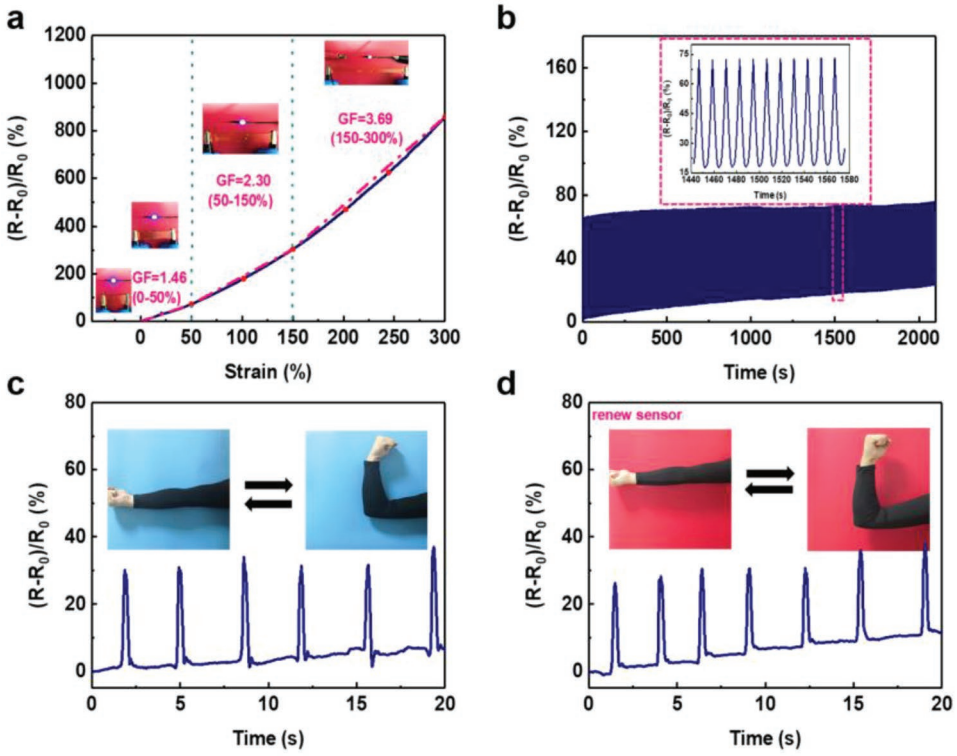

Figure 4. Strain sensing behavior of the polymer composite (with 0.1 mol% Fe^{3+}). a) Relative resistance changes versus strain up to 300%. b) Relative resistance changes versus test time during cyclic tensile loading up to a fixed strain of 50% for 250 cycles. c,d) Relative resistance changes versus test time for polymer composite (c, original material; d, recycled material) as sensor to detect the straightening and bending of the elbow joint.

3.69 within 300% strain, respectively, indicating that this polymer composite possesses satisfactory sensitivity with a large strain sensing range. This finding may be caused by the weak hydrogen bonding interaction between ionic parts (CCl) and the carboxylic groups of the molecular chains. When the strain was applied on the polymer composite, the deformation of the molecular chains facilitated the movements of positive/negative ions. Thus, the resistance changes could be obviously found in the polymer composite. In addition, this composite exhibited no measurable degeneration of the output signal after enduring 250 cycles of 50% strain (Figure 4b). This indicated the good repeatability of our polymer composites acting as sensing materials.

To further illustrate the feasibility of the polymer composites in application of electronic devices, we used them as ionic conductor to fabricate wearable soft strain sensors for detecting various human motions. For example, the fabricated strain sensor was attached to elbow and detect the elbow joint motion with evident resistance changes with applied strain (Figure 4c). This is because the strain could result in the deformation of the polymer composite, which further broke the ionic pathway, leading to a significant resistance increase suddenly. When the elbow joint was completely straightened, the resistance immediately recovered to their original state. The cycling test indicated this sensor possesses very good repeatability for bending of the elbow joint. As shown in Figure S24 (Supporting Information), the different resistance variation can be observed as the forefinger bended to different angles (from 30° to 90°). Moreover, due to the outstanding electrical stability of our composites, the captured sensing signal could be constant while keeping the forefinger at a certain angle (Figure S25, Supporting Information). Meanwhile, Figure S26 (Supporting Information) showed the relative resistance variation strain sensor attached on opisthenar with different directions, which could track, distinguish the different state of motion according to the output sensing signal, indicating the good sensing reliability of our strain sensors. Instead of detecting large-scale human activities, the strain sensor could be used to monitor subtle motions. For example, we mounted the sensor to volunteer's chest and detected the normal physiological breathing in a relaxed state (Figure S27, Supporting Information), showing obvious and repeatable output signals with inhalation and exhalation. The sensing behaviour of our polymer composite to pressure was also investigated, as shown in Figure S28 (Supporting Information). The current increased abruptly to different levels with the pressure progressively increased from 50 to 150 kPa. This may be due to the fact that pressure is conducive to shorten the conductive pathway, thus leading to the obvious variation of the current. Along with the repeated pressure for two times, moreover, the current values recorded are nearly invariable. They could finally return to their original state in a short time after the applied pressure disappears.

2.5. Full Recyclability

Among various functional materials, interest is increasing exponentially in the development of fully recyclable materials for electronic device applications. In this work, our polymer

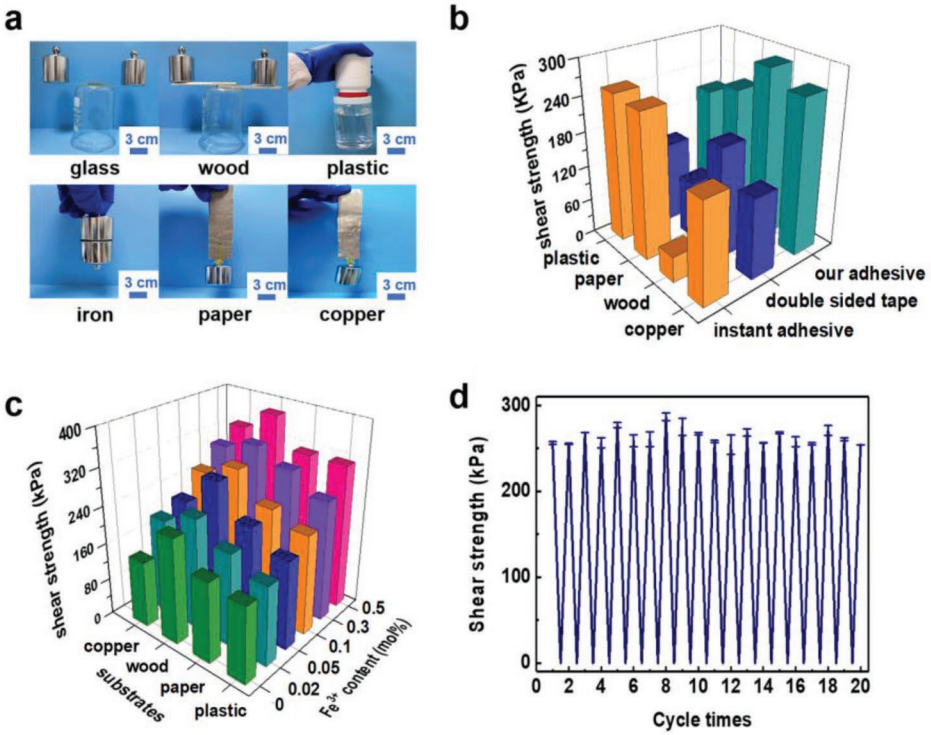

Figure 5. Adhesion behavior of the recycled polymer composite adhesives. a) Digital images of adhesion behavior of the adhesive on various surfaces. b) Comparison of adhesion strength between our adhesive and instant adhesive, double side tape on surfaces of plastic, paper, wood, and copper. c) Adhesion strength of the adhesives with different Fe^{3+} content on the copper, wood, paper, and plastic surfaces. d) The adhesion strength of the adhesive on wood surface after 20 times cycles.

composites could be fully recycled when it suffers damage or is not used anymore. The used polymer composites could be easily molten into homogeneous solution by a direct heating process, which could be reused for making new ionic conductors and adhesives (Figure S29, Supporting Information). As a step toward confirming the fully recyclable property, the strain sensors based on new ionic conductor were attached to elbow joint (Figure 4d), forefinger (Figure S30, Supporting Information), and opisthenar (Figure S31, Supporting Information) for detecting their motions. The corresponding patterns of resistance curves were similar to that of the virgin ones, which suggested the recycling does not have noticeable impact on sensing performance of our polymer composites. Furthermore, the used composites can also be recycled and reprocessed into adhesives.[38] We found this adhesive had excellent adhesion to various surfaces (**Figure 5**a). This can be attributed to the reproduction of polymer networks between the paralleled surfaces after cooling. The tensile adhesive test was conducted to quantify the adhesion strength of our adhesives to the related surfaces. As shown in Figure 5b, the highest adhesion strengths were 208 kPa for plastic, 232 kPa for paper, 289 kPa for wood, and 264 kPa for copper, respectively. The adhesive strength to wood is higher than that to other substrates. It is mainly due to the tough formation of hydrogen bonds between carboxylic groups of the polymer composite and hydroxyl groups of the wood. Meanwhile, we compared the adhesion strength of instant adhesive, double side tape with our adhesive. The adhesion strength of adhesive for copper surface is higher than that of instant adhesive and double side tape. This result probably resulted from the formation of the metal complexation between the composite and copper surface.[34] Additionally, we elucidated the effects of the Fe^{3+} content on adhesion strength of our adhesive for copper, wood, paper, and plastic surfaces (Figure 5c). With an increase of Fe^{3+} content, the adhesion strengths for copper, wood, paper, and plastic surfaces were all improved, suggesting that the Fe^{3+} content plays an important role for improvement of the adhesion strength. As demonstrated in Figure 5d, this adhesive also showed repeatable adhesion to wood surface, with almost no distinct variation in adhesion strength.

3. Conclusion

In summary, novel multifunctional polymer composites based on LA were developed through constructing a hierarchical polymer networks consisting of disulfide bonds, hydrogen bonds, and coordination bonds. The solvent-free process is extremly facile, fast, low-cost, and especially, based on biological available materials. Taking advantage of the hierarchical networks, the as-fabricated polymer composites possess excellent light transmittance (>85%), ultrahigh stretchability (strain up to 1100%), and excellent self-healing capability (mechanical healing efficiency of 86%, electrical healing efficiency of 96%), which render them perfect candidates to be used as ionic conductors for various functional applications. Moreover, these materials exhibit outstanding strain sensitivity and good repeatability,

which are able to detect various human activities such as joint motion and breathing. Impressively, these polymer composites can be fully recycled and reprocessed into new ionic conductors or adhesives by a direct heating process, which has rarely been demonstrated in other ionic conductors. Owing to their smart structure and excellent features, these polymer composites are promising, sustainable, and functional materials to further investigate and introduce to the field of advanced sensors and actuators.

4. Experimental Section

Materials: α-Lipoic acid (LA, 99%), choline chloride (CCl, 98%), acrylic acid (AA, > 99%) were obtained by Shanghai Macklin Biochemical Co. Ltd., China. Ferric chloride ($FeCl_3$) were purchased from Beijing Lanyi Co. Ltd., China.

Materials Synthesis: The polymer composites were prepared through one-step polymerization. Initially, LA (10 g) monomer was heated at 90 °C and vigorously stirred for 30 min until a yellow transparent liquid was obtained. Then, AA (3 g) was added dropwise, and the mixture was maintained at the same conditions for 10 min. CCl (2 g) was then introduced into the mixture liquid and stirred vigorously for 10 min. Finally, $FeCl_3$ (0.02–0.5%, molar ratio compared with the sum of LA and AA) was dissolved in the mixture liquid under the same heating and stirring for 10 min. The resultant mixture liquid was poured into circular mold for allowing the mixture liquid to cool down at room temperature, thus obtaining the resultant polymer composites. The polymer composites without Fe^{3+} were fabricated by the similar method.

Wearable Strain Sensors Fabrication: The polymer composite with a size of $5 \times 1 \times 0.5$ cm^3 as ionic conductors to prepare wearable strain sensors was used. Two Cu wires as electrodes were connected on both sides of the composite. Subsequently, the polymer composite was fixed onto the volunteer's elbow joint, forefinger, and opisthenar by using commercial tapes to sense the motions.

Recycling Process: The recycling process only needs to simply heat the used polymer composite at 90 °C for 30 min for melting the polymer composite matrix into low-viscosity liquid. Subsequently, the recycled liquid is poured into mold and a new, functional ionic conductor is obtained after cooling to room temperature. Alternatively, the recycled liquid can also be deposited on a substrate for usage in adhesive. After the deposition, another substrate was put on the deposited recycling liquid, followed by cooling to adhere the two substrates.

General Characterization: The Raman spectra, Fourier transform infrared (FT-IR) spectra, UV–vis absorption spectra, Analysis (TGA), and Differential scanning calorimetry (DSC) were recorded by LabRAM Aramis Raman spectrometer, Bruker Vertex 33 spectrometer, Cary 5000 spectrophotometer, NETZSCH tester, and 214 polyma NETZSCH tester, respectively. The transmittance was evaluated by utilizing Agilent Cary60 UV–vis spectrophotometer. The rheological measurement was conducted by using TA AR2000 rheometer. Frequency sweep was performed at a constant strain of 0.1% by varying frequency 0.01 to 100 rad s^{-1} at 25 °C. The dynamic strain sweep was measured at a frequency of 6.28 rad s^{-1}. The tensile tests were carried out utilizing a tensile machine (INSTRON 5565, 500N load cell). Each sample was cut into a strip (2×4 cm^2) for testing. The conductivity of the polymer composites was measured at 25 °C and 35% relative humidity through EIS measurement. The measuring instrument was CHI660E Electrochemical workstation underwent the current ranging of 200 mA, and the frequency range from 1 Hz to 1 MHz. The sample was cut into pieces 5 mm (width) × 5 mm (length) × 1 mm (thickness) and sandwiched by copper tapes. The voltage of the current test for pressure sensor is 1 V. The conductivity was calculated by (1)[54]

$$\rho^{-1} = L/(s \times R) = L/(s \times Z') \quad (1)$$

where ρ is the resistivity of sample, L is the effective length of sample pieces, s means the cross-sectional area of sample, R means the resistance of sample, and Z' is the real part of impedance of sample. The real-time resistance characteristics for all strain sensors were recorded by DMM7501 Digital Graphical Sampling Multimeter (Keithley Instrument USA), and the output voltage for determining the resistance is 3.6 V. The sample was cut into pieces 5 cm (width) × 1 cm (length) × 5 mm (thickness) and sandwiched by copper tapes. The adhesives were employed to the surface of the wood, paper, plastic, and copper with a fixed bonding area of 3 cm × 2.5 cm, respectively. Adhesive tests were performed to evaluate the adhesion strength by using tensile machine (INSTRON 5565, 500N load cell).

Supporting Information

Supporting Information is available from the Wiley Online Library or from the author.

Acknowledgements

The authors are grateful for the financial support for this work by the National Natural Science Foundation of China (21774036), Guangdong Province Science Foundation (2017B090903003, 2017GC010429).

Conflict of Interest

The authors declare no conflict of interest.

Keywords

adhesive, full recyclability, ionic conductor, strain sensor, α-lipoic acid

Received: March 26, 2019
Revised: May 6, 2019
Published online:

[1] Q. Li, Z. Ullah, W. W. Li, Y. F. Guo, J. B. Xu, R. B. Wang, Q. Zeng, M. L. Chen, C. J. Liu, L. W. Liu, *Small* **2016**, *12*, 5058.
[2] Y. J. Liu, W. T. Cao, M. G. Ma, P. B. Wang, *ACS Appl. Mater. Interfaces* **2017**, *9*, 25559.
[3] K. H. Kim, N. S. Jang, S. H. Ha, J. H. Cho, J. M. Kim, *Small* **2018**, *14*, 1704232.
[4] F. Xu, X. Wang, Y. T. Zhu, Y. Zhu, *Adv. Funct. Mater.* **2012**, *22*, 1279.
[5] A. E. Aliev, J. Oh, M. E. Kozlov, A. A. Kuznetsov, S. L. Fang, A. F. Fonseca, R. Ovalle, M. D. Lima, M. H. Haque, Y. N. Gartstein, M. Zhang, A. A. Zakhidov, R. H. Baughman, *Science* **2009**, *323*, 1575.
[6] D. H. Kim, N. S. Lu, R. Ma, Y. S. Kim, R. H. Kim, S. D. Wang, J. Wu, S. M. Won, H. Tao, A. Lalam, K. J. Yu, T. Kim, R. Chowdhury, M. Ying, L. Z. Xu, M. Li, H. J. Chung, H. Keum, M. McCormick, P. Liu, Y. W. Zhang, F. G. Omenetto, Y. G. Huang, T. Coleman, J. A. Rogers, *Science* **2011**, *333*, 838.
[7] D. J. Lipomi, M. Vosgueritchian, C. K. B. Benjamin, S. L. Hellstrom, J. A. Lee, C. H. Fox, Z. N. Bao, *Nat. Nanotechnol.* **2011**, *6*, 788.
[8] F. Ding, H. Ji, Y. Chen, A. Herklotz, K. Dorr, Y. Mei, A. Rastelli, O. G. Schmidt, *Nano Lett.* **2010**, *10*, 3453.
[9] B. Meng, W. Tang, Z. H. Too, X. S. Zhang, M. D. Han, W. Liu, H. X. Zhang, *Energy Environ. Sci.* **2013**, *6*, 3235.

[10] H. C. Ko, M. P. Stoykovich, J. Z. Song, V. Malyarchuk, W. M. Choi, C. J. Yu, J. B. Geddes III, J. L. Xiao, S. D. Wang, Y. G. Huang, J. A. Rogers, *Nature* **2008**, *454*, 748.
[11] G. Shi, Z. H. Zhao, J. H. Pai, L. Lee, L. Q. Zhang, C. Stevenson, K. Lshara, R. J. Zhang, H. W. Zhu, J. Ma, *Adv. Funct. Mater.* **2016**, *26*, 7614.
[12] J. Ge, H. B. Yao, X. Wang, Y. D. Ye, J. L. Wang, Z. Y. Wu, J. W. Liu, F. J. Fan, H. L. Gao, C. L. Zhang, S. H. Yu, *Angew. Chem.* **2013**, *125*, 1698.
[13] J. A. Fan, W. H. Yeo, Y. Su, Y. Hattori, W. Lee, S. Y. Jung, Y. H. Zhang, Z. J. Liu, H. Y. Cheng, L. Falgout, M. Bajema, T. Coleman, D. Gregoire, R. J. Larsen, Y. G. Huang, J. A. Rogers, *Nat. Commun.* **2014**, *5*, 3266.
[14] S. W. Chun, Y. H. Choi, W. J. Park, *Carbon* **2017**, *116*, 753.
[15] X. L. Wang, T. J. Li, J. Adams, J. Yan, *J. Mater. Chem. A* **2013**, *1*, 3580.
[16] M. Park, J. Park, U. Jeong, *Nano Today* **2014**, *9*, 244.
[17] G. F. Cai, J. X. Wang, K. Qian, J. W. Chen, S. H. Li, P. S. Lee, *Adv. Sci.* **2017**, *4*, 1600190.
[18] T. Yamada, Y. Hayamizu, Y. Yamamoto, Y. Yomogida, A. Izadi-Najafabadi, D. N. Futaba, K. Hata, *Nat. Nanotechnol.* **2011**, *6*, 296.
[19] Y. Y. Zhang, C. J. Sheehan, J. Y. Zhai, G. F. Zou, H. M. Luo, J. Xiong, Y. T. Zhu, Q. X. Jia, *Adv. Mater.* **2010**, *22*, 3027.
[20] Y. Y. Huang, E. M. Terentjev, *Adv. Funct. Mater.* **2010**, *20*, 4062.
[21] N. S. Lu, C. Lu, S. X. Yang, J. Rogers, *Adv. Funct. Mater.* **2012**, *22*, 4044.
[22] Y. R. Jeong, H. Park, S. W. Jin, S. Y. Hong, S. S. Lee, J. S. Ha, *Adv. Funct. Mater.* **2015**, *25*, 4228.
[23] Y. Wang, L. Wang, T. T. Yang, X. Li, X. B. Zang, M. Zhu, K. L. Wang, D. H. Wu, H. W. Zhu, *Adv. Funct. Mater.* **2014**, *24*, 4666.
[24] J. Lee, S. Kim, J. Lee, D. Yang, B. C. Park, S. Ryu, L. Park, *Nanoscale* **2014**, *6*, 11932.
[25] F. Xu, Y. Zhu, *Adv. Mater.* **2012**, *24*, 5117.
[26] S. S. Yao, Y. Zhu, *Adv. Mater.* **2015**, *27*, 1480.
[27] X. G. Yu, Y. Q. Li, W. B. Zhu, P. Huang, T. T. Wang, N. Hu, S. Y. Fu, *Nanoscale* **2017**, *9*, 6680.
[28] X. Jing, H. Y. Mi, Y. J. Lin, E. Enriquez, X. F. Peng, L. S. Turng, *ACS Appl. Mater. Interfaces* **2018**, *10*, 20897.
[29] A. R. Li, G. X. Chen, M. H. He, J. F. Tian, B. Su, *J. Mater. Chem. C* **2017**, *5*, 8475.
[30] J. Y. Sun, C. Keplinger, G. M. Whitesides, Z. Suo, *Adv. Mater.* **2014**, *26*, 7608.
[31] D. Y. Choi, M. H. Kim, Y. S. Oh, S. H. Jung, J. H. Jung, H. J. Sung, H. W. Lee, H. M. Lee, *ACS Appl. Mater. Interfaces* **2017**, *9*, 1770.
[32] Z. W. Wang, H. W. Zhu, J. L. Lai, B. Yan, H. B. Liu, X. L. Jin, A. J. Ma, G. Zhang, W. F. Zhao, W. X. Chen, *J. Mater. Chem. C.* **2018**, *6*, 9200.
[33] Y. Wang, S. Gong, S. J. Wang, G. P. Simon, W. L. Chen, *Mater. Horiz.* **2016**, *3*, 208.
[34] C. Y. Shao, M. Wang, L. Meng, H. L. Chang, B. Wang, F. Xu, J. Yang, P. B. Wang, *Chem. Mater.* **2018**, *30*, 3110.
[35] B. H. Chen, J. J. Lu, C. H. Yang, J. H. Yang, J. X. Zhou, Y. M. Chen, Z. Suo, *ACS Appl. Mater. Interfaces* **2014**, *6*, 7840.
[36] M. S. Kim, J. Y. Park, C. Namkoong, P. J. Jang, J. W. Ryu, H. S. Song, J. Y. Yun, I. S. Namgoong, J. Ha, I. S. Park, I. K. Lee, B. Viollet, J. H. Youn, H. K. Lee, K. U. Lee, *Nat. Med.* **2004**, *10*, 727.
[37] X. Zhang, R. M. Waymouth, *J. Am. Chem. Soc.* **2017**, *139*, 3822.
[38] Q. Zhang, C. Y. Shi, D. H. Qu, Y. T. Long, B. L. Feringa, H. Tian, *Sci. Adv.* **2018**, *4*, eaat8192.
[39] W. J. Chung, J. J. Griebel, E. T. Kim, H. Yoon, A. G. Simmonds, H. J. Ji, P. T. Dirlam, R. S. Glass, J. J. Wie, N. A. Nguyen, B. W. Guralnick, J. Park, A. Somogyi, P. Theato, M. E. Mackay, Y. E. Sung, K. Char, J. Pyun, *Nat. Chem.* **2013**, *5*, 518.
[40] Y. M. Xin, H. Peng, J. Xu, J. Y. Zhang, *Adv. Funct. Mater. 29*, **2019**, 1808989.
[41] Y. L. Rao, A. Chortos, R. Pfattner, F. Lissel, Y. C. Chiu, V. Feig, J. Xu, T. Kurosawa, X. Gu, C. Wang, M. Q. He, J. W. Chung, Z. N. Bao, *J. Am. Chem. Soc.* **2016**, *138*, 6020.
[42] Q. H. Zhang, K. D. O. Vigier, S. Royer, F. Jerome, *Chem. Soc. Rev.* **2012**, *41*, 7108.
[43] D. Carriazo, M. C. Serrano, M. C. Gutierrez, M. L. Ferrer, F. Monte, *Chem. Soc. Rev.* **2012**, *41*, 4996.
[44] M. H. Liao, P. B. Wang, J. R. Wen, M. Gong, X. X. Wu, Y. G. Wang, R. Shi, L. Q. Zhang, *Adv. Funct. Mater.* **2017**, *27*, 1703852.
[45] P. Podsiadlo, A. K. Kaushik, E. M. Arruda, A. M. Waas, B. S. Shim, J. Xu, H. Nandivada, B. G. Pumplin, J. Lahann, A. Ramamoorthy, N. A. Kotov, *Nature* **2007**, *318*, 80.
[46] T. J. Trivedi, D. Bhattacharjya, J. S. Yu, A. Kumar, *ChemSusChem* **2015**, *8*, 3294.
[47] C. Y. Shao, H. L. Chang, M. Wang, F. Xu, J. Yang, *ACS Appl. Mater. Interfaces* **2017**, *9*, 28305.
[48] J. Y. Sun, X. H. Zhao, W. R. K. Illeperuma, O. Chaudhuri, K. H. Oh, D. J. Mooney, J. J. Vlassak, Z. G. Suo, *Nature* **2012**, *489*, 133.
[49] Y. Y. Zhang, S. S. Gong, Q. Zhang, P. Ming, S. J. Wan, J. S. Peng, L. J. Jiang, Q. F. Cheng, *Chem. Soc. Rev.* **2016**, *45*, 2378.
[50] T. Wang, Y. Zhang, Q. C. Liu, W. Cheng, X. R. Wang, L. J. Pan, B. X. Xu, H. X. Xu, *Adv. Funct. Mater.* **2018**, *28*, 1705551.
[51] P. Cordier, F. Tournilhac, C. S. Ziakovic, L. Leibler, *Nature* **2008**, *451*, 977.
[52] N. Roy, B. Bruchmann, J. M. Lehn, *Chem. Soc. Rev.* **2015**, *44*, 3786.
[53] B. C. K. Tee, C. Wang, R. Allen, Z. N. Bao, *Nat. Nanotechnol.* **2012**, *7*, 825.
[54] M. Wang, R. A. Li, G. X. Chen, S. H. Zhou, X. Feng, Y. A. Chen, M. H. He, D. T. Liu, T. Song, H. S. Qi, *ACS Appl. Mater. Interfaces* **2019**, *11*, 14313.

